J Solid State Electrochem (2015) 19:1151–1160
DOI 10.1007/s10008-014-2699-1

ORIGINAL PAPER

Enhanced photovoltaic and photoelectrocatalytic properties by free-standing TiO_2 nanotubes via anodization

Juanru Huang · Xin Tan · Tao Yu · Lin Zhao · Hang Liu

Received: 15 August 2014 / Revised: 29 November 2014 / Accepted: 2 December 2014 / Published online: 10 January 2015

Abstract This work employs a simple anodization to develop free-standing TiO_2 nanotubes with controllable sizes via a self-detaching technique, and the resulting close-bottom-up free-standing TiO_2 nanotubes are faced Degussa P25 particle film, precoated on a fluorine-doped SnO_2 conductive glass, to fabricate a TiO_2 composite. The resulting composites, whose sizes can be controlled by modulating the reanodizing time, were used as the photoanode films and oxidative catalyst to investigate their corresponding photoelectrochemical properties. Compared with P25 particle film, these resulting composites reveal the improved photocatalytic and photovoltaic performance, which results from the effective transfer of photo-generated charges by these characteristic nanotubular arrays. The composite, based on the free-standing TiO_2 nanotubes (~10.88 μm), indicates the highest photovoltaic conversion efficiency (7.64 %) under a standard AM 1.5 solar simulator and degradation rate (95.20 %) under the UV irradiation of 75 min, and these results are probably attributed by the positive synergistic effect of the transport of photo-generated charges, the diffusion path of reactants, and the penetration length of incident light into films in comparison to other free-standing TiO_2 nanotubes. In addition, the higher photoelectrocatalytic activity is acquired by electrochemically assisted photocatalytic degradation.

Keywords TiO_2 nanotubes · Anodization · Photocatalytic · Photoanode

J. Huang · T. Yu (✉) · L. Zhao
School of Chemical Engineering and Technology, Tianjin University, Tianjin 300072, China
e-mail: yutao@tju.edu.cn

J. Huang · L. Zhao · H. Liu
School of Environmental Science and Engineering, Tianjin University, Tianjin 300072, China

X. Tan
School of Science, Tibet University, Lhasa City 850000, China

T. Yu
Tianjin University-National Institute for Materials Science (TU-NIMS) Joint Research Center, Tianjin University, Tianjin 300072, China

Introduction

One-dimensional TiO_2 nanotubes (TNTs), which are fabricated by anodizing a Ti substrate, have been significantly attracted because of their low cost, photochemical stability, environmental friendliness, and unique nanotubular structure. These structured properties facilitate photo-generated electron transport and then reduce charge recombination compared to conventional TiO_2 nanoparticle film. Since Grimes et al. first reported the growth of TNT arrays on anodized Ti substrates in electrolytes such as HF [1], the influence factors of TNT growth, such as electrolyte composition [2], work voltage [3–5] and current [3], reaction time [4, 6] and temperature [6, 7], and electrode materials [8], have been widely investigated. Up to date, their corresponding applied investigations on photocatalysis [4, 9–11], dye-sensitized solar cells (DSSCs) [12], water splitting [13], sensors and transducers [2, 14], nanostructure templates and drug release platform [15], and nanocapacitors [16] have been consequently conducted, and the results showed that these materials exhibited some amazing properties. However, conventional TNTs grown on an opaque Ti substrate has already limited their wider application. For instance, these TNTs, which are used as the photoanode films, only require a back-illuminated DSSC and thus result in a less photovoltaic conversion efficiency, the probable reasons are attributed to the incident light

adsorption and reflection by the photoanode and electrolyte [17], and the trap-limited diffusion pattern by photo-generated electron transport [18]. In addition, TiO_2 barrier layer between TNT arrays and a Ti substrate aggravates photo-generated charge recombination [19, 20] or/and obstructs molecular diffusion [21–23].

Therefore, several techniques [21–31] have been developed to fabricate free-standing TNTs (FS-TNTs), and subsequently, these FS-TNTs are integrated or attached on any foreign substrates by adhesion layer of TiO_2 particle paste or sol [17, 20, 32, 33], as these configurations have already showed the fascinating properties in photovoltaic [17, 18, 31, 33–36] and catalytic [25, 29, 30, 37–39] applications. In 2006, Grimes group [33] fabricated the DSSC based on the anodizing presputtered Ti layers on a transparent FTO substrate as the photoanode, and then achieved the photovoltaic conversion efficiency of 2.90 %, but these lower TNTs and corresponding expensive procedure largely limited its further investigation. In the meantime, FS-TNTs by stripping TNTs from a Ti substrate was first reported and used in flow-through photocatalysis with a very high efficiency [30], the subsequent techniques of mechanical delamination [21, 22, 25, 26], chemical dissolution [19, 20, 30, 31, 34, 38], and reactive conditions [6, 27, 40, 41] are performed to remove TNTs from Ti substrates, and the corresponding investigations evidently indicate that these resulting FS-TNTs can promote photo-generated electron transport, facilitate electron collection, and then improve their photoelectrochemical performance [19, 30, 38]. Besides, FS-TNTs also display other functional properties in some applied fields [21].

Recently, the front-illuminated DSSCs with the close-bottom-up (CBU) FS-TNTs facing TiO_2 nanoparticles (CBU FS-NPs, configuration) exhibit an enhanced photovoltaic properties than those of the front-illuminated cells based on the open-top-up (OTU) FS-NPs (OTU FS-NPs, configuration) [31, 35] and the corresponding back-illuminated cells based on TNTs on a Ti substrate [19]. The characteristic nanotubular structures can effectively promote the photo-generated carrier transport [18, 31, 42, 43] in the photoanode and, thus, improve their photovoltaic conversion efficiency, and the CBU FS-NP configuration reveals the improvement in suppression photo-generated electron/hole recombination compared to a conventional TiO_2 nanoparticle film. Nevertheless, few reports comprehensively focus on the effect of FS-TNTs with controllable sizes on their relevant catalytic and photovoltaic properties.

In this work, FS-TNTs with controllable sizes were synthesized according to our previous work [6] and were further characterized via FE-SEM, FE-TEM with EDX, XRD, XPS. The as-synthesized FS-TNTs were transferred to a pretreatment FTO substrate by using a thin layer of P25 (anatase and rutile TiO_2) particle paste as the "adhesive," and the resulting TiO_2 composite was used as the photoanode and a catalysis to investigate their photovoltaic and catalytic properties, respectively. The investigations indicate that the length of TNTs, the transport of reactants, and the penetration length of incident light into films cooperatively contributed to the improved photovoltaic and catalytic performance of resulting FS-P25 composites.

Experimental section

Fabrication of FS-TNTs

Vertically oriented and self-detaching FS-TNTs with controllable sizes were fabricated via three-step anodization and following by heat treatment [6]. Prior to anodization, Ti substrates were orderly washed using anhydrous ethanol, isopropanol, and distilled water for 10 min in an ultrasonic bath. The anodizing process at a direct current of 60 V was conducted in a two-electrode electrochemical cell containing Ti substrates (0.5 mm, 1 cm × 4 cm, 99.7 %) as the work electrode, Pt wire (99.7 %) as the counter electrode, and ethylene glycol electrolyte with 0.5 wt.% NH_4F and 3.0 vol.% tri-distilled water. First, cleaned Ti substrates were anodized for 30 min at room temperature, and then, the anodized substrates were ultrasonically treated to remove these as-formed TNT layers. Next, the pretreated Ti substrates were used as the templates and implemented the reanodizing reaction with the time of 1, 2, 3, and 4 h, and subsequently, these substrates were put into the muffle furnace and annealed at 450 °C in air for 2 h with a temperature ramp of 2 °C/min. Last, the annealed TNT arrays on a Ti substrate were tri-anodized in the original electrolyte of 45 °C and then were peeled off from the as-forming amorphous TiO_2 film on this substrate during this tri-anodizing treatment, and this process lasted about 15 min, and then, the detached TNTs were reannealed at 250 and 450 °C for 1 h. Corresponding to the reanodized time of 1, 2, 3, and 4 h, these detached TNTs were labeled as FS1-TNTs, FS2-TNTs, FS3-TNTs, and FS4-TNTs (see Table 1), respectively.

Table 1 These anodizing films with characteristic parameters

Film	Reanodizing time (h)	Temperature (°C)	Length (μm)
P25 film	0	450	9.50±0.08
FS1-TNTs	1	450	7.10±0.05
FS2-TNTs	2	450	10.88±0.06
FS3-TNTs	3	450	13.93±0.08
FS4-TNTs	4	450	19.58±0.06

FS-P25 composites

Fluorine-doped SnO_2 conductive glasses (thickness of 2.2 mm, NSG, Japan) with a size of 2.0 cm×2.0 cm were bathed in ultrasonic ethanol, isopropanol, and thrice-distilled water for 5 min after they were bathed in a detergent solution for 15 min, and then, these substrates were dried in the oven. The substrates were pretreated with 40-mM $TiCl_4$ solution at 70 °C and further printed with a P25 particle paste containing 6 g of P25, 16 mL of absolute ethanol, 0.1 mL of acetic acid, 0.6 g of polyethylene glycol (PEG-600, Aldrich), 2 g of ethocel (Aldrich) via a doctor-blading technique. The preprepared FS-TNTs were transferred on a precoated P25 paste (as the adhesive between FS-TNTs and substrates) on the substrates (marked FS-P25 composite, see Fig. 1) under a slight pressure with a slide glass. These resulting TiO_2 composites were annealed from 125 to 450 °C, similar to the method by Gräztel et al. [44]. When the heat treatment had cooled down to 120 °C, these composites were taken out and quickly put into the same $TiCl_4$ solution to keep for 30 min. Subsequently, they were separately rinsed with thrice-distilled water and annealed at 450 °C for 30 min. According to FS1-TNTs, FS2-TNTs, FS3-TNTs, and FS4-TNTs, these composites were marked as FS1-P25, FS2-P25, FS3-P25, and FS4-P25 (see Table 1) composite, respectively.

DSSC fabrication

When the above treatment was dropped to 120 °C, the annealed composites immediately immersed into 30 μM of N719 (DYESOLD Limited) solution in a mixture of acetonitrile and *tert*-butanol (vol=1:1) for 30 h to 32 h to ensure complete sensitizer uptake, the redundant dyes over these composite were washed with the mixture solution and dried at room temperature under the dark. The sensitized photoanode composites (active area 0.80 cm×0.80 cm) were sandwiched with Pt photocathode (1.20 cm×1.80 cm, Heptachroma, China), which was already pretreated in an ultrasonic absolute alcohol for 10 min, separated by 60 μm of surlyn1702 (Solaronix, Switzerland) spacer. The space was filled with the high-performance electrolyte DHS-E23 (Heptachroma, China). Similar to the front-illuminated DSSCs, P25 paste was used to fabricate the reference cell and was further investigated.

Characterization and measurement

FS-TNTs were characterized via FE-SEM (5.0 kV, S4800), FE-TEM with EDX (CuKa, 200 kV, Tecnai G2 F20), and XRD (Rigaku D/max 2500v/pc, CuKa). The bond energy of FS-TNTs and TNT with Ti substrate was measured via XPS (PHI1600). The thickness of P25 particle films was measured using a surface morphology instrument (DEKTAK6M, VEECO). The photocurrent-potential (*J-V*) measurements of DSSCs were performed using a Keithley 2400 digital source meter controlled by a computer and a standard AM 1.5 solar simulator (300 W, Oriel 91160-1000 SOLAR SIMULATOR 2×2 BEAM), which was calibrated by an Oriel reference solar cell. The monochromatic incident photon-to-electron conversion efficiencies (*IPCE*) of DSSCs were determined using a commercial setup (QTest Station 2000 IPCE Measurement System, CROWNTECH, USA).

Photoelectrocatalytic performance

Photocatalytic (PC) degradation was performed in a homemade quartz reactor with a water cooling jacket and an arc xenon lamp (HSX-F300, 300 W, Beijing NBelt Technology CO., Ltd., China) along with collimated, filtered light ($CuSO_4$ filter, λ=365 nm). The aligned samples were vertically placed into this reactor containing 100 mL of 10 mg/L methylene blue (MB) aqueous solution containing 0.1 M NaCl solution (supporting electrolyte) and fixed a distance of 28.0 cm from the light source with the irradiating intensity (10.0 mW/cm^2) measured by a spectroradiometer (USR-40; Ushio Inc., Japan). Before the degradation, N_2 was introduced into the reactor to keep the MB solution homogenous, and the degradation solution was kept in the dark for 30 min to maintain the

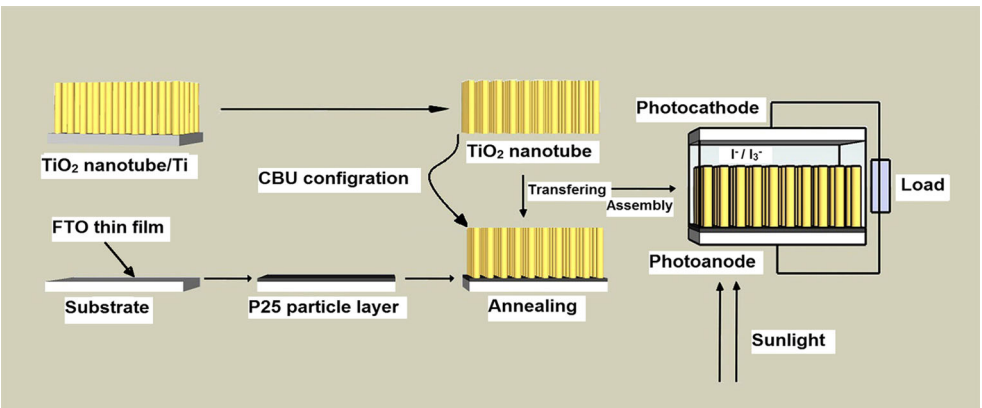

Fig 1 Schematic diagram of assembling DSSCs based on FS-TNTs

MB absorption-desorption equilibrium. The MB concentration was measured every 15 or 30 min by using a UV-Vis spectrophotometer (T6, PERSEE, China) at an intensity of 665 nm during the process.

The photoelectrocatalytic (PEC) and electrocatalytic (EC) degradation were implemented in the same solution using a three-electrode configuration with a resulting TiO_2 composite as a photoanode, saturated Ag/AgCl as a reference electrode, and a Pt silk as a counter electrode, and the pH of this solution was regulated to be 5.0 by 1 M HCl or NaOH solution. A scanning potentiostat (CH Instruments, model CH 660E) was used to provide the applied voltage (0.5 V) for PEC and EC degradation.

Results and discussion

Fabrication of the FS-TNT films

FS-TNTs were fabricated by anodizing a Ti substrate at a direct current of 60 V [6]. Based on FE-SEM measurements, FS-TNTs with an open top and a closed bottom are shown in Fig. 2a–b. With the reanodizing time, their corresponding length is extended and labeled in Fig. 2c–f, and all samples executed three time to measure their thicknesses via FE-SEM, and their measurement errors are listed in Table 1. FS2-TNTs are also characterized via FE-TEM with EDX, and the inner diameter and outer diameter of FS2-TNTs are denoted in Fig. 2g, and Ti, O species were further detected for the sample in Fig. 2h.

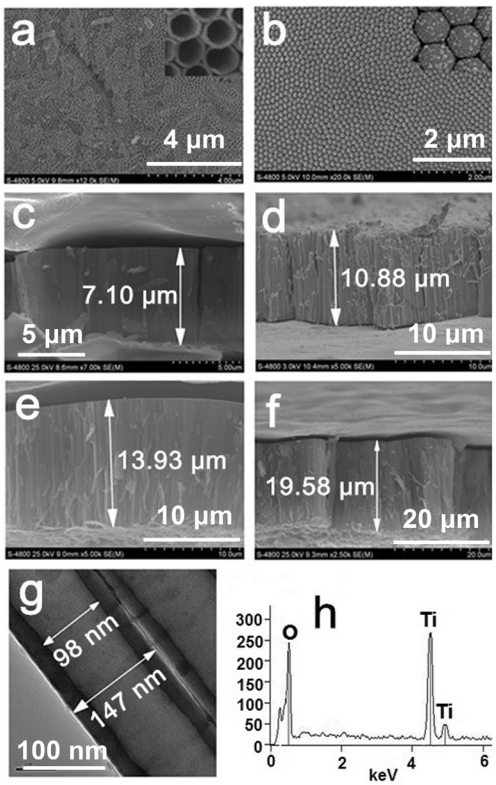

Fig. 2 *Top* (**a**) and *bottom* (**b**) FE-SEM images of the FS2-TNT film, the *insets* show magnified *top* and *bottom* images, respectively. Cross-section FE-SEM images of these resulting composites annealed at 450 °C. FE-TEM image (**g**) of FS2-TNTs based on EDX measurement (**h**)

To confirm the crystalline and crystal planes of FS-TNTs, FS2-TNTs annealed at 250 and 450 °C were characterized via XRD and FE-TEM with electron diffraction, as shown in Fig. 3. The curve A and curve B indicate the XRD spectra of FS2-TNTs annealed at 250 and 450 °C, respectively. Compared with JCPDS (No. 21-1272), the sample sintered at 250 °C is almost amorphous except for a weak characteristic peak of (101) plane in the curve A, and the peaks at 450 °C are indexed to (101), (004), (200), (105), (211), (204), (116), (200), (215), (214) planes of anatase TiO_2 in the curve B. In Fig. 3b–c, the selected area electron diffraction (SAED) of FS-TNTs is indexed to the polycrystalline anatase TiO_2, which is consistent with the result of XRD.

To further investigate their chemical states, FS2-TNTs annealed at 450 °C were measured via XPS measurement, and the full spectra (a), C1s (b), O1s (c), Ti2p (d) binding energy are shown in Fig. 4. The C1s (~284.7 eV) peak of Fig. 4a stems from the measurement correction of standard C1s (~284.7 eV) and/or the carbonization of the residual electrolyte. Compared with O1s at ~530.0 eV of the standard spectra [45], O1s at ~529.7 eV of Fig. 4c slightly deviate the standard, which is probably caused by chemical configuration, and further confirms the Ti–O bond at TiO_2 [46, 47]. $Ti2p_{3/2}$ at

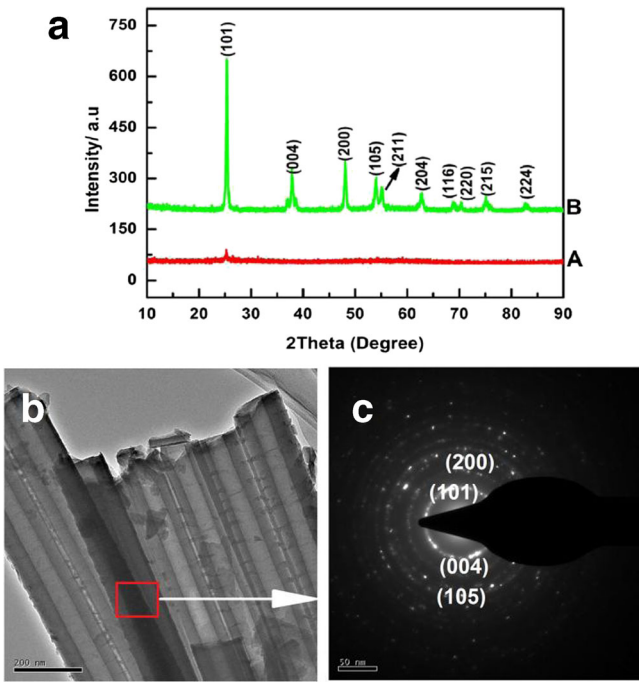

Fig. 3 **a** XRD spectra of FS2-TNTs annealed at 250 °C (*A*) and 450 °C (*B*). **b** FE-TEM image of FS2-TNT film annealed at 450 °C and **c** selected reagion for electron diffraction

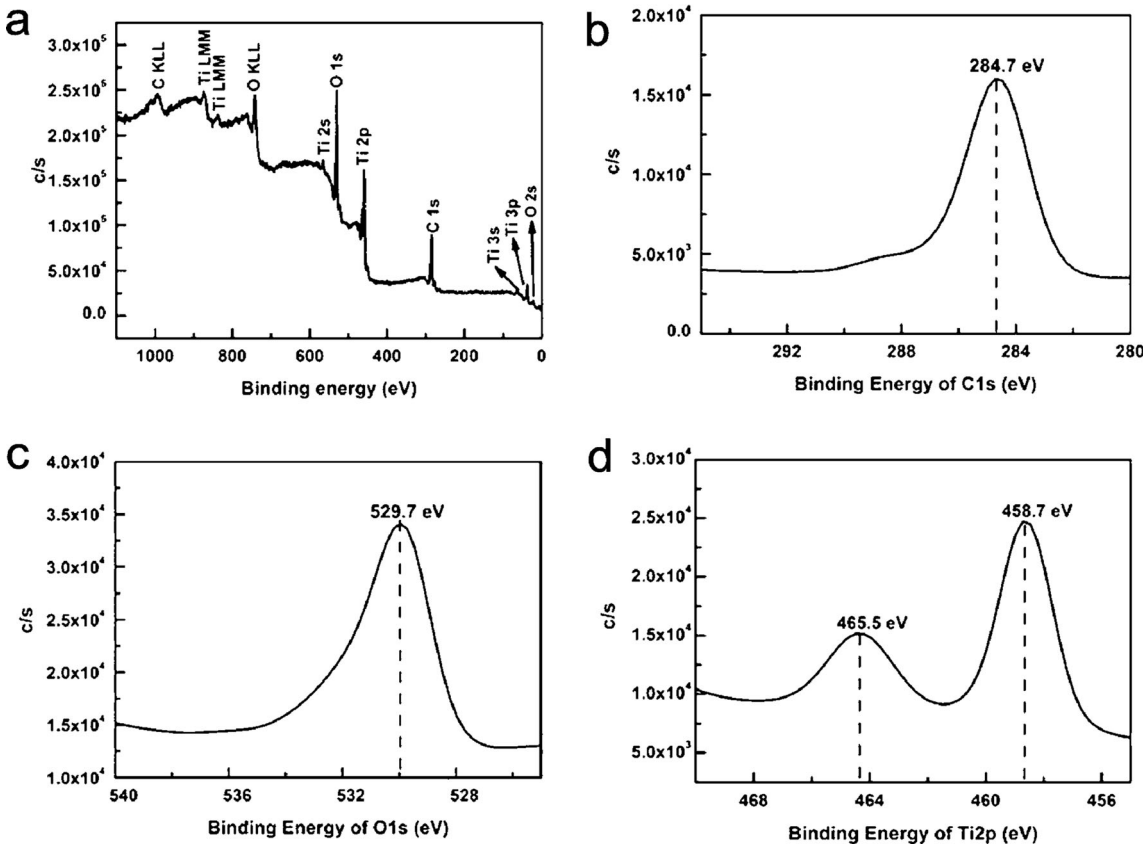

Fig. 4 XPS full spectra (**a**) and C1s (**b**), O1s (**c**), Ti2p (**d**) binding energies of FS2-TNTs annealed at 450 °C

~458.7 eV and $Ti2p_{1/2}$ at ~465.5 eV of Fig. 4d also deviate from the standard $Ti2p_{3/2}$ at ~458.0 eV and $Ti2p_{1/2}$ at ~464.0 eV [45], respectively, which are also attributed to the chemical configuration [46, 47].

Photovoltaic properties

Based on the previous work [6, 31], FS-P25 CBU configuration displayed the better contact properties between TNTs and P25 particle film than OTU FS-P25 configuration. Accordingly, the cell with CBU configuration exhibited better contact properties, higher photovoltaic efficiency, greater charge transfer resistance from the interface of FTO/TiO_2 to the electrolyte, and more dye loading than the cell with OTU configuration [31]. Furthermore, the cell with FS-TNTs facing the TiO_2 particle film also displayed an improvement over the corresponding back-illuminated DSSC with TNTs on an opaque Ti substrate [18, 35]. Before the fabrication of DSSC with a FS-P25 CBU configuration, the cell with FS-TNTs signifies a larger photovoltaic efficiency (η) in comparison to P25-based cell in our previous work[6]. Therefore, CBU configuration in this work was fabricated by combining FS-TNTs with P25 particle film. Based on FS-TNTs, the front-illuminated DSSC with an FS-P25 CBU configuration is fabricated in Fig. 1.

The *J-V* and *IPCE* curves of Fig. 5a–b show that shout-circuit current (J_{sc}), open-circuit voltage (V_{oc}), fill factor (*FF*), η, and *IPCE* of CBU-based DSSCs are higher than those of the corresponding P25-based DSSC, and the results are probably attributed to the significant increase of electron lifetime and diffusion length for the CBU-based cells by the unique nanotubular structure [17]. Their specific photovoltaic parameters of DSSCs are shown in Table 2. Compared to the photovoltaic properties of P25-based cell, the CBU-based cells exhibit the powerfully enhanced photovoltaic performance. With the length of FS-TNTs from ~7.10 μm to ~10.88 μm, ~13.93 μm and ~19.58 μm, J_{sc} gradually increases from 15.03 mA/cm^2 to 15.64 mA/cm^2 and 17.93 mA/cm^2 and then decreases to 13.73 mA/cm^2. The thicker TNTs first facilitate the photo-generated electron transport by unique nonotubular and improve light-harvesting efficiency by more dye loading, then the further prolongation probably sharply decreases the intensity of incident light penetration to reduce light-harvesting and, thus, produces additional length of photo-generated charge transport to enhance the dark current [48] and subsequently reduce the value of J_{sc} [18, 42]. The corresponding V_{oc} gradually reduces from the peak value of 759.00 to 704.00 mV with the more length of TNTs, which may be caused by the augmentative surface area and

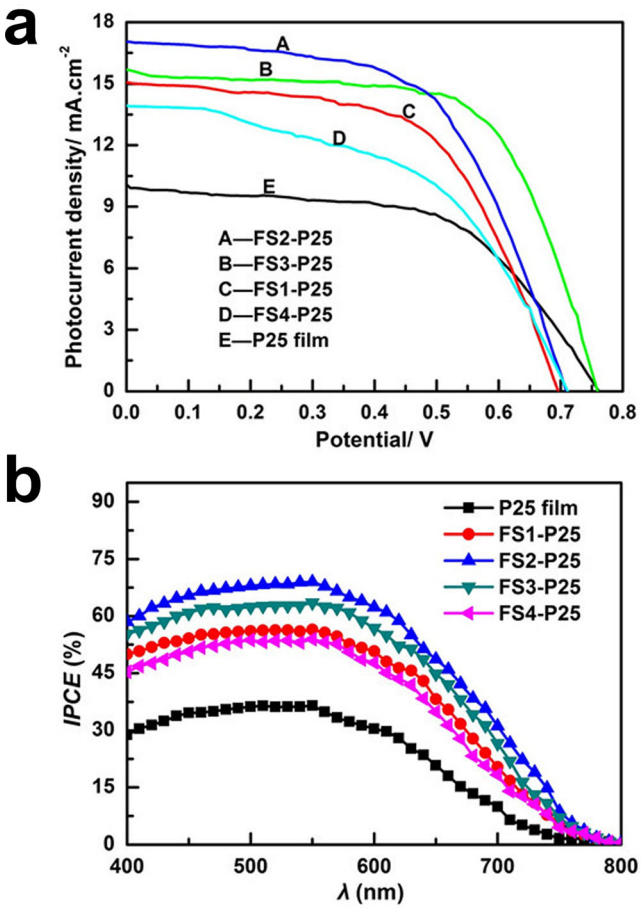

Fig. 5 *J-V* (**a**) and *IPCE* (**b**) curves of the front-illuminated DSSCs based on the CBU FS-P25 configuration and P25 film.

following additional recombination sites of electron/hole pairs. The longer TNTs have larger surface areas to adsorb more dye molecules and then improve incident light harvesting to generate more photo-generated electrons. On the other hand, more length of TNTs with the more dyes cannot contribute to the light harvest because the thickness of solid film severely attenuate the light penetration [49], and inversely weaken the transport mechanism of these carriers by redundant TNTs and loading dye. Furthermore, the diffusion and photo-excitation of dye molecules are affected by the thickness of film and light intensity [49], respectively. The above results indicate that the length of TNTs, adsorbing reactants, and incident light penetration synergistically determined the photovoltaic performance and the CBU-based cells, based on FS2-TNTs, exhibit the optimal photovoltaic efficiency (η= 7.64 %). In addition, the subsequent *IPCE* characteristic is also shown in Fig. 5b, and the *IPCE* values of FS-P25 composites are bigger than those of P25 film. With the length of FS-TNTs, the *IPCE* value of FS-P25 composites with the wavelength (λ) from 400 to 800 nm show the same trend of η, and the peak value of *IPCE* is approximately 69.00 % at λ=550 nm for FS2-P25 composite.

Photoelectrocatalytic properties

PEC and corresponding PC and EC properties of these FS-P25 composites were evaluated, and their degradation results and corresponding fitting curves of reaction kinetics are shown in Figs. 6, 7, and 8. Before the degradation, these adsorption-desorption processes were performed to keep the adsorption equilibrium of MB molecules over composites [50], the adsorption decoloration, PEC and PC degradation are shown in Figs. 6a and 7a (A, B indicates the decoloration from the adsorption and degradation, respectively). The slight decoloration occurs in the adsorption and degradation of blank, and the decoloration of PEC, PC adsorption is less than 3.00 % in comparison to their degradation (see Table 3); thus, the adsorption of MB over composites is neglected in the following degradation. In Figs. 6b and 7b, PEC and PC degradation rate of MB gradually increases with the irradiation time, and their data are listed in Table 3. Compared to P25 film, the activities of FS-P25 composites are distinctly enhanced, and FS2-P25 composite displays the highest rates in PEC and PC degradation, which are probably attributed to the optimal thickness and their structured features [51, 52]. With the increase of TNT length, the longer TNTs can load more MB molecules to improve light harvesting and, meanwhile, extend the diffusion length of photo-generated charges, and the opposite trend is also brought because the incident light intensity penetrates into the extending film. With the extension over one certain value, the extending TNTs probably provide more recombination sites of photo-generated electron/hole pairs by weakening light

Table 2 The photovoltaic properties of FS-TNT-based DSSCs

Photoanode	Loading N719 (10^{-8}mol/cm^{-2})	J_{sc} (mA/cm^2)	V_o (mV)	*FF*	η (%)
P25 film	15.85±1.10	10.88±0.12	735.00±13	0.60±0.03	4.78±0.23
FS1-P25	22.45±1.62	15.03±0.10	689.00±10	0.59±0.01	6.12±0.13
FS2-P25	25.47±1.56	15.64±0.15	759.00±15	0.64±0.02	7.64±0.24
FS3-P25	29.05±1.52	17.93±0.09	705.00±12	0.56±0.02	7.06±0.20
FS4-P25	31.25±1.58	13.73±0.12	704.00±12	0.52±0.03	5.00±0.22

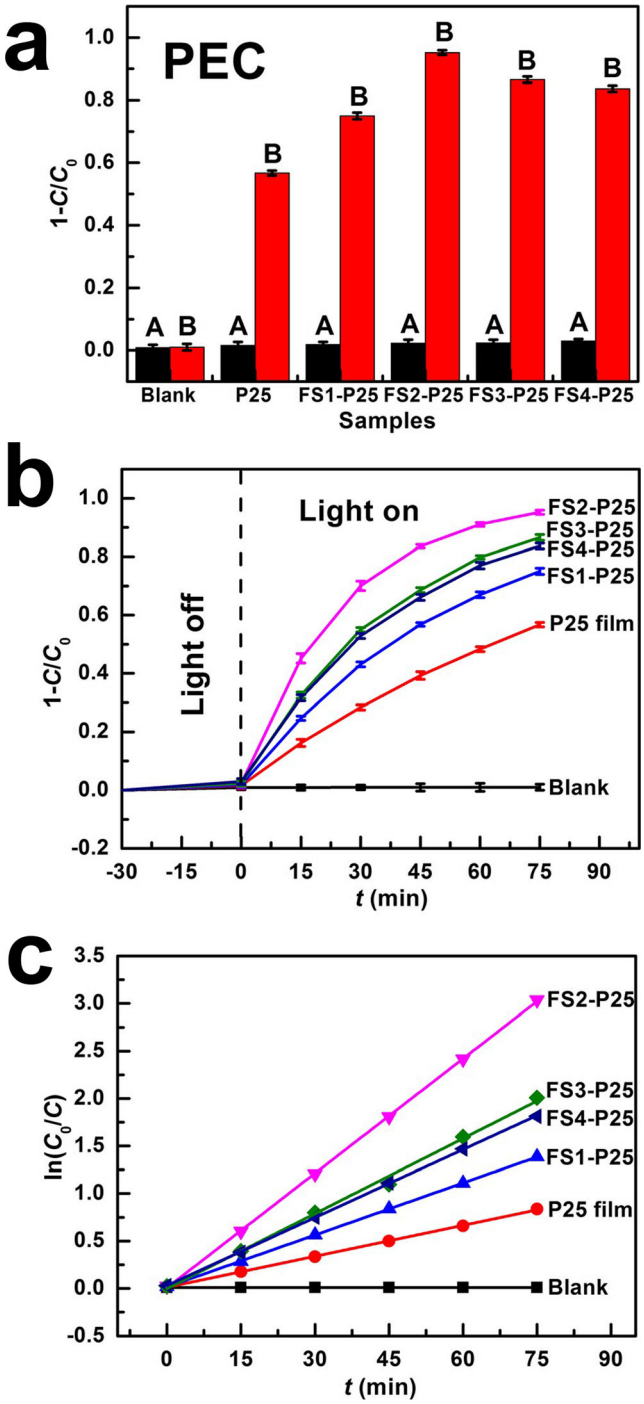

Fig. 6 **a** The adsorption-desorption equilibrium and PEC process of these composites and reference P25 film. *Blank A* and *B* indicate the adsorption-desorption equilibrium and PEC process, respectively. **b–c** PEC properties of these composites, reference P25 film, blank and the corresponding pseudo-first-order PEC kinetics

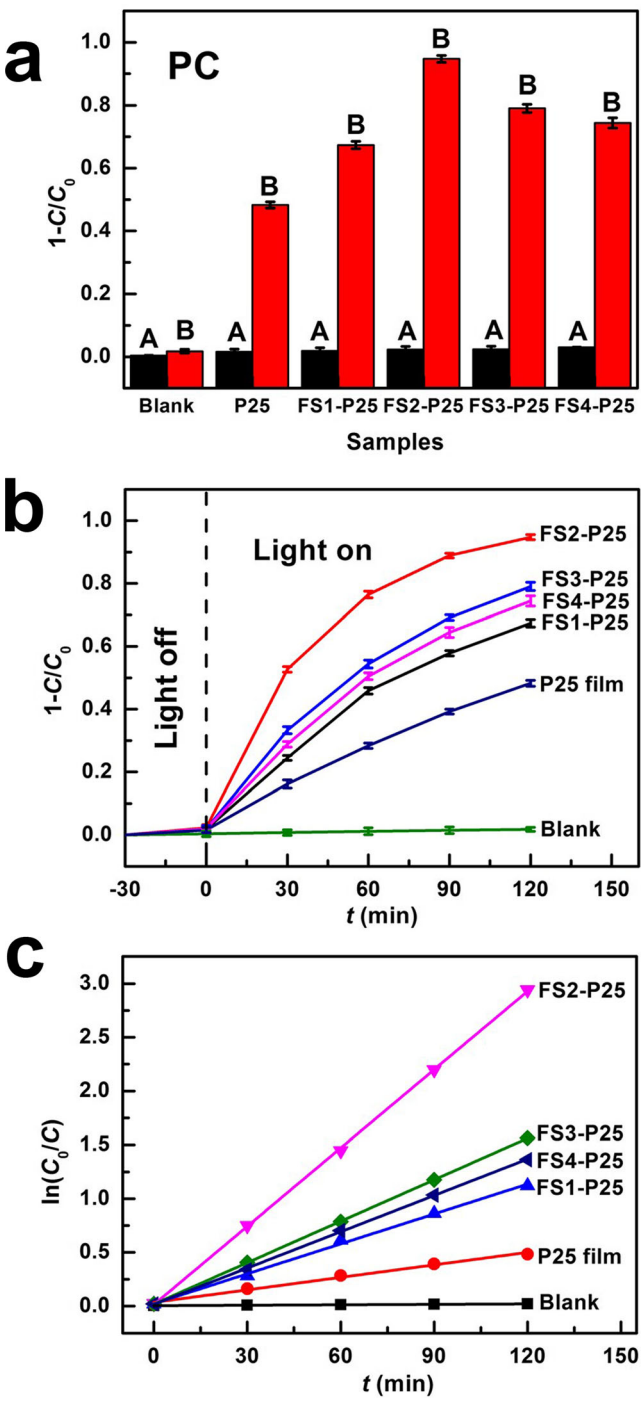

Fig. 7 **a** The adsorption-desorption equilibrium and PC process of these composites and reference P25 film. *Blank A* and *B* indicate the adsorption-desorption and PC process, respectively. **b–c** PC properties of these composites, P25 film, blank and the corresponding pseudo-first-order PC kinetics

intensity and reactant diffusion [49], and thus, less carriers participate in the degradation to decrease the reactive rate [51, 53]. In addition, the nanotubular features effectively accelerate the photo-generated charges transport and reduce the gain boundary to improve their rates in comparison to P25 film.

To determine the kinetics of catalytic reaction, the linear-relationship fitting curves of the degradation versus the corresponding irradiation time are shown in Figs. 6c and 7c. The dye degradation rate can be depicted by the Langmuir-Hinshelwood mechanism as follows:

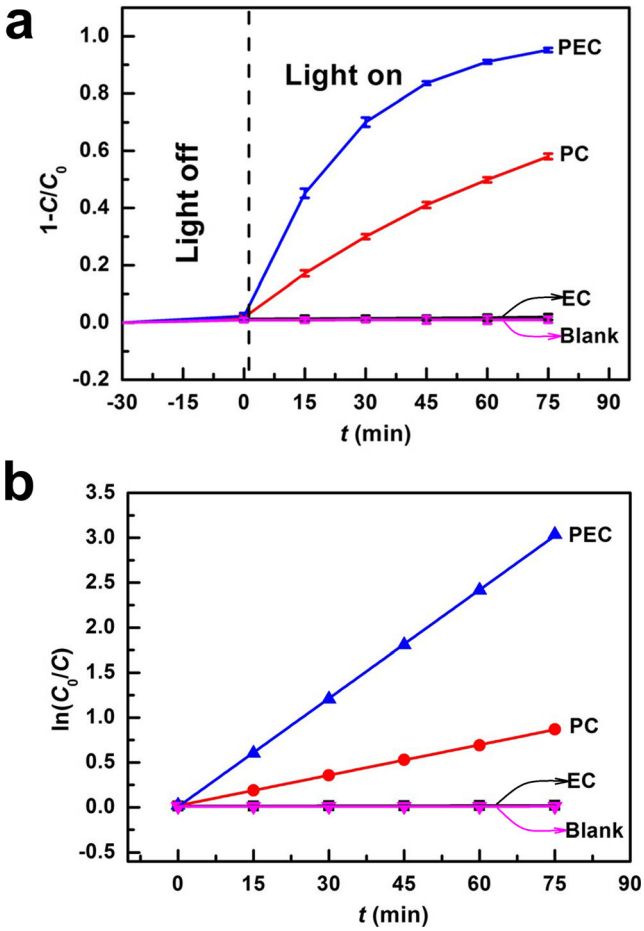

Fig. 8 **a** PEC, PC, EC activities of FS2-P25 composite and blank (PEC) with the irradiation time from −30 to 75 min. **b** Their corresponding pseudo-first-order kinetics

$$r = \mathrm{d}C/\mathrm{d}t = kKC/(1 + KC) \quad (1)$$

where r represents the initial rate of photo-oxidation, C is the concentration at t, k' is the reaction rate constant, and K is the dye adsorption coefficient on the catalyst. If the dye concentration is low enough, the pseudo-first-order reaction conditions can apply, and KC is very small compared with 1 in the denominator of Eq. 1. Thus, Eq. 1 can be simplified as follows

$$lnC/C_0 = kKC = kt \quad (2)$$

where $k=k'K$ is the pseudo-first-order reaction constant and C_0 is the initial dye concentration. Based on the degradation of FS-P25 composites and P25 film, the reactions are fitted into the pseudo-first-order reaction to decolorize MB solution under the irradiation, as shown in Figs. 6c and 7c. Accordingly, these rate constants of FS-P25 composites are clearly larger than those of P25 film (see Table 3), which indicates that FS-P25 composites reveal the higher activities, and their matching rate constants are listed in Table 3. The highest PEC and PC constants are accomplished by FS2-P25 composite in the degradation. Besides, PEC, PC, and EC activities of FS2-P25 composite with the irradiation time of 75 min are also implemented to investigate the coupling effect of PC and EC degradation in Fig. 8, and their corresponding data of degradation and first-order reaction fitting are listed in Table 4. The result indicates that PEC degradation rate is higher than PC, EC degradation, which is described to intensify photo-generated charge separation by external applied voltage when these composites are excited under UV irradiation.

Compared with P25 film, FS-P25 composites exhibit the improved catalytic properties, and the highest photovoltaic efficiency and degradation rate are further achieved by FS2-P25 film based on FS2-TNTs. With the first increase of TNT length, the longer TNTs adsorb more MB molecules to improve light harvesting, and the positive diffusion of reactants also distinctly accelerates the photo-generated carrier transport on TNTs; these results cooperatively enhance the photovoltaic efficiency and degradation rate. With the further extension over the given length, however, redundant TNTs provide more photo-generated charges recombining sites and less dyes loading than the former by the attenuation of reactant diffusion, and also leads to weaken the penetration of incident light into TNTs. As a result, the length of TNTs, diffusion path of reactants, and light penetration are collectively contributed to the photovoltaic and catalytic properties. In addition, PEC degradation is caused by the coupling mechanism of the PC and EC operation.

Table 3 PEC, PC, adsorption docoloration of the resulting composites and reference P25 film

Catalysis	PC adsorption	PC degradation	k of PC (min^{-1})	PEC adsorption	PEC degradation	k of PEC (min^{-1})
Blank	0.39 %	1.99 %	1.32694 E^{-4}	0.91 %	1.01 %	1.34857 E^{-4}
P25 film	1.59 %	48.28 %	0.00388	1.58 %	56.69 %	0.01089
FS1-P25	1.86 %	67.37 %	0.00928	1.84 %	75.05 %	0.01827
FS2-P25	2.29 %	94.73 %	0.02429	2.32 %	95.20 %	0.04022
FS3-P25	2.66 %	79.04 %	0.01286	2.68 %	86.58 %	0.02634
FS4-P25	2.99 %	74.43 %	0.01127	2.96 %	83.68 %	0.02388

Table 4 The adsorption decoloration and degradation of FS2-P25 composite and Blank (PEC)

Parameters	FS2-P25	Blank	*k* of FS2-P25 (min^{-1})
PEC adsorption	2.29%	0.91%	–
PEC degradation	95.20%	1.01%	0.04022
PC adsorption	1.84%	–	–
PC degradation	58.04%	–	0.01129
EC adsorption	1.26%	–	–
EC degradation	1.97%	–	9.04729 E^{-5}

Conclusion

FS-TNTs with controllable sizes are synthesized via three-step anodization, and their structural features, crystal phase, and chemical constitution are further characterized, and FS-P25 composites and the corresponding DSSCs are also fabricated based on the above FS-TNTs. The photovoltaic measurement and PEC, PC, EC degradation draw conclusions: (1) FS-TNT sample with the length of tubes 10.88 micros is characterized with the highest photovoltaic efficiency 7.64 %, comparing with value 4.78 for P25 film. (2) The composite, based on FS-TNT sample with the value 10.88, displays the improved PEC and PC activities by the degradation of MB solution, and the highest rate is 95.20 % for PEC degradation and 94.73 % for PC degradation over this composite. (3) With the increase of TNT length, the catalytic degradation and photovoltaic efficiencies first increase and then decrease, the probable reasons are attributed to the synergistic effect of the length of TNTs, the reactant diffusion and the penetration length of incident light into films.

Acknowledgments This work was supported by National Basic Research Program of China (973 program, No. 2012CB720100, No. 2014CB239300), National Natural Science Foundation of China (No. 21406164, 21466035), and Science Foundation of Ministry of Education of China (No. 20130032120019, No. 20110032110037).

References

1. Gong D, Grimes CA, Varghese OK, Hu WC, Singh RS, Chen Z, Dickey EC (2001) J Mater Res 16:3331–3334
2. Su ZX, Zhou WZ (2011) J Mater Chem 21:8955–8970
3. Li LL, Tsai CY, Wu HP, Chen CC, Diau EWG (2010) J Mater Chem 20:2753–2819
4. Sreekantan S, Saharudin KA, Lockman Z, Tzu TW (2010) Nanotechnology 21:365603
5. Gui Q, Yu D, Zhang S, Xiao H, Yang C, Song Y, Zhu X (2014) J Solid State Electron 18:141–148
6. Huang JR, Tan X, Yu T, Zhao L, Xue S (2012) Rsc Adv 2:12657–12660
7. Xie ZB, Blackwood DJ (2010) Electrochim Acta 56:905–912
8. Yang Y, Lee K, Kado Y, Schmuki P (2012) Electrochem Commun 17:56–59
9. In SI, Nielsen MG, Vesborg PCK, Hou Y, Abrams BL, Henriksen TR, Hansen O, Chorkendorff I (2011) Chem Commun 47:2613–2615
10. Huang JR, Tan X, Yu T, Zhao L (2014) Electrochim Acta 146:278–287
11. Huang JR, Tan X, Yu T, Zhao L, Xue S, Hu WL (2014) J Mater Chem A 2:9975–9981
12. Agarwala S, Ho GW (2012) J Solid State Chem 189:101–107
13. Allam NK, Shankar K, Grimes CA (2008) J Mater Chem 18:2341–2348
14. Feng C, Xu G, Liu H, Lv J, Zheng Z, Wu Y (2014) J Solid State Electron 18:163–171
15. Song YY, Schmidt-Stein F, Bauer S, Schmuki P (2009) J Am Chem Soc 131:4230–4232
16. Dumitriu C, Pirvu C, Demetrescu I (2013) J Electrochem Soc 160: G55–G60
17. Lamberti A, Sacco A, Bianco S, Manfredi D, Cappelluti F, Hernandez S, Quaglio M, Pirri CF (2013) Phys Chem Chem Phys 15:2596–2602
18. Hsiao PT, Liou YJ, Teng HS (2011) J Phys Chem C 115:15018–15024
19. Chen QW, Xu DS (2009) J Phys Chem C 113:6310–6314
20. Lin CJ, Yu WY, Chien SH (2010) J Mater Chem 20:1073–1077
21. Chen QQ, Xu DS, Wu ZY, Liu ZF (2008) Nanotechnology 19: 365708
22. Meng X, Lee TY, Chen H, Shin DW, Kwon KW, Kwon SJ, Yoo JB (2010) J Nanosci Nanotechnol 10:4259–4265
23. Paulose M, Prakasam HE, Varghese OK, Peng L, Popat KC, Mor GK, Desai TA, Grimes CA (2007) J Phys Chem C 111: 14992–14997
24. Paulose M, Peng LL, Popat KC, Varghese OK, Latempa TA, Bao TA, Desai TA, Grimes CA (2008) J Memb Sci 319:199–205
25. Ng JW, Zhang XW, Zhang T, Pan JH, Du JHA, Sun DD (2010) J Chem Technol Biotechnol 85:1061–1066
26. Singh S, Festin M, Barden WRT, Xi L, Francis JT, Kruse P (2008) ACS Nano 2:2363–2373
27. Jo Y, Jung I, Lee I, Choi J, Tak Y (2010) Electrochem Commun 12: 616–619
28. Wang DA, Liu LF (2010) Chem Mater 22:6656–6664
29. He XL, Cai YY, Zhang HM, Liang CH (2011) J Mater Chem 21:475–480
30. Albu SP, Ghicov A, Macak JM, Hahn R, Schmuki P (2007) Nano Lett 7:1286–1289
31. Dubey M, Shrestha M, Zhong Y, Galipeau D, He H (2011) Nanotechnology 22:285201
32. Varghese OK, Paulose M, Grimes CA (2009) Nat Nanotechnol 4: 592–597
33. Mor GK, Shankar K, Paulose M, Varghese OK, Grimes CA (2006) Nano Lett 6:215–218
34. Park JH, Lee TW, Kang MG (2008) Chem Commun 25:2867–2869
35. Li LL, Chen YJ, Wu HP, Wang NS, Diau EWG (2011) Energ Environ Sci 4:3420–3425
36. Qiu JJ, Zhuge FW, Lou K, Li XM, Gao XD, Gan XY, Yu WD, Kim HK, Hwang YH (2011) J Mater Chem 21:5062–5068
37. Liao J, Lin S, Pan N, Li S, Cao X, Cao Y (2012) Mater Charact 66: 24–29
38. Lin CJ, Yu WY, Lua YT, Chien SH (2008) Chem Commun 45:6031–6033
39. Lin CJ, Yu YH, Liou YH (2009) Appl Catal B-Environ 93:119–125
40. Lin J, Chen JF, Chen XF (2010) Electrochem Commun 12:1062–1065
41. Kant K, Losic D (2009) Phys Status Solidi-R 3:139–141
42. Lei BX, Liao JY, Zhang R, Wang J, Su CY, Kuang DB (2010) J Phys Chem C 114:15228–15233
43. Gao X, Chen J, Yuan C (2013) J Power Sources 240:503–509
44. Ito S, Murakami TN, Comte P, Liska P, Grätzel C, Nazeeruddin MK, Grätzel M (2008) Thin Solid Films 516:4613–4619
45. Liu F, Zhao ZJ, Qiu LM, Zhao LZ (2009) AnanlysisTest Technol Instrum (In Chinese) 15(1):1–17

46. Wang D, Xiao L, Luo Q, Li X, An J, Duan Y (2011) J Hazard Mater 192:150–159
47. Hamal DB, Klabunde KJ (2011) J Phys Chem C 115:17359–17367
48. Kuang DB, Ito S, Wenger B, Klein C, Moser JE, Humphry-Baker R, Zakeeruddin SM, Grätzel M (2006) J Am Chem Soc 128:4146–4154
49. Chang HT, Wu NM, Zhu FQ (2000) Water Res 34:407–416
50. Xiong L, Yang Y, Mai J, Sun W, Zhang C, Wei D, Chen Q, Ni J (2010) Chem Eng J 156:313–320
51. Liu ZY, Zhang XT, Nishimoto S, Murakami T, Fujishima A (2008) Environ Sci Technol 42:8547–8551
52. Zhang XM, Huo KF, Hu LS, Wu ZW, Chu PK (2010) J Am Ceram Soc 93:2771–2778
53. Liang HC, Li XZ (2009) J Hazard Mater 162:1415–1422